

Evolution of coherent collective modes through consecutive CDW transitions in $(\text{PO}_2)_4(\text{WO}_3)_{12}$ mono-phosphate tungsten bronze

L. Stojchevska,¹ M. Borovšak,^{1,2} P. Foury-Leylekian,³ J.-P. Pouget,³ T. Mertelj,^{1,4,*} and D. Mihailovic^{1,2,4}

¹Complex Matter Department, Jozef Stefan Institute, Jamova 39, 1000 Ljubljana, Slovenia

²Faculty of Mathematics and Physics, University of Ljubljana, Jadranska 19, 1000 Ljubljana, Slovenia

³Laboratoire de Physique des Solides, UMR CNRS 8502, Université Paris Sud, 91405 Orsay - France

⁴Center of Excellence on Nanoscience and Nanotechnology Nanocenter

(CENN Nanocenter), Jamova 39, 1000 Ljubljana, Slovenia

(Dated: September 11, 2018)

All optical femtosecond relaxation dynamics in a single crystal of mono-phosphate tungsten bronze $(\text{PO}_2)_4(\text{WO}_3)_{2m}$ with alternate stacking $m = 6$ of WO_3 layers was studied through the three consequent charge density wave (CDW) transitions. Several transient coherent collective modes associated to the different CDW transitions were observed and analyzed in the framework of the time dependent Ginzburg-Landau theory. Remarkably, the interference of the modes leads to an *apparent rectification* effect in the transient reflectivity response. A saturation of the coherent-mode amplitudes with increasing pump fluence well below the CDWs destruction threshold fluence indicates a decoupling of the electronic and lattice parts of the order parameter under strong optical drive.

I. INTRODUCTION

Time-resolved spectroscopy can give unique insight in the dynamical behaviour of the elementary excitations in systems undergoing charge density wave (CDW) transitions. The appearance of new collective vibrational excitations in Raman¹⁻³ and coherent transient reflectivity⁴⁻⁶ response upon charge density wave (CDW) formation is well documented¹⁻⁷ and theoretically quite well understood.⁷ In systems with more than one CDW transition new collective modes are expected to appear below each transition temperature, as observed experimentally in the Raman response^{2,3}. In the transient reflectivity response^{6,8}, however, the additional coherent oscillation modes below the subsequent CDW transition temperatures have not been readily observed. Investigating the differences in the response associated with different transitions gives important information on the coupling and damping of collective modes, and behaviour of the order parameter in each case.

The mono-phosphate tungsten bronzes $(\text{PO}_2)_4(\text{WO}_3)_{2m}$ are an example of low dimensional CDW materials⁹ offering a possibility to further explore the effect of consecutive CDW transitions on the transient-reflectivity coherent oscillatory response. They are quasi two-dimensional (2D) conductors built from layers of WO_6 octahedra parallel to the (a, b) -plane and separated by PO_4 tetrahedra¹⁰⁻¹³ as shown in Fig. 1. Their electronic properties arise from quasi-one-dimensional chain structures where - due to the strong Fermi surface nesting - charge-density-wave (CDW) instabilities develop below certain critical transition temperatures T_{CDW} , as confirmed by various experimental techniques^{10,14,15}. For $(\text{PO}_2)_4(\text{WO}_3)_{2m}$ with $m = 6$ in particular three CDW transitions have been observed: $T_{\text{CDW1}} = 120$ K, $T_{\text{CDW2}} = 62$ K and $T_{\text{CDW3}} = 30$ K^{9,10,16}.

Up to date, a substantial effort has been put into study-

ing the electronic, magnetic and structural properties of $(\text{PO}_2)_4(\text{WO}_3)_{2m}$ bronzes,¹⁷⁻¹⁹ however, to the best of our knowledge there is no Raman or time-resolved optical spectroscopy study of the sequence of CDW phases in $(\text{PO}_2)_4(\text{WO}_3)_{2m}$ tungsten bronzes. In this paper we therefore report on temperature and fluence dependence of the transient reflectivity in a mono-phosphate tungsten bronze $(\text{PO}_2)_4(\text{WO}_3)_{2m}$ single crystal with $m = 6$ ($\text{P}_4\text{W}_{12}\text{O}_{44}$) on a femtosecond time scale, focusing on the effect of the subsequent CDW transitions on the coherent oscillatory transient response.

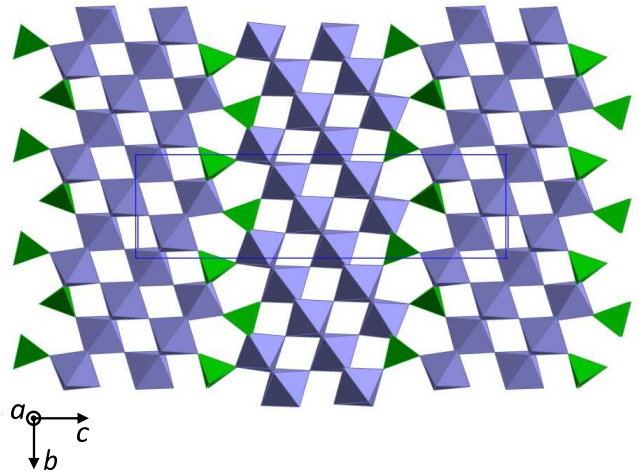


Figure 1. Crystal structure of $(\text{PO}_2)_4(\text{WO}_3)_{12}$ showing the WO_6 octahedra and the mono-phosphate PO_4 tetrahedra projected along the a crystallographic direction.

II. EXPERIMENTAL

Single crystals used in this study were grown at CRISMAT (Caen, France) according to a previously reported method.²⁰ They have a shape of platelets with large surface of about $(1 \times 1.5) \text{ mm}^2$, corresponding to the (a, b) conducting plane, and a thickness of $\sim 1/10 \text{ mm}$ along c . The index $m = 6$ of the bronze was unambiguously determined by the measurement of the inter-slab periodicity¹¹ c ($c = 23.57$ for $m = 6$).

Optical experiments were performed with 50 fs laser pulses at 800 nm generated from an amplified Ti:Sapphire mode-locked laser at a 250 kHz repetition rate. The transient reflectivity $\Delta R/R = \frac{R_p - R_0}{R_0}$, where R_p and R_0 are the reflectivities in the absence and presence of the pump pulse, respectively, was monitored using a standard pump-probe technique where both pump and probe photons were at 1.55 eV photon energy. The beam diameters on the sample were determined by means of calibrated pinholes to be $108 \text{ }\mu\text{m}$ and $50 \text{ }\mu\text{m}$ for the pump and probe beam, respectively. Both beams were perpendicularly polarized to each other and oriented relatively to the crystal axes in a way to obtain maximum/minimum response amplitude at low temperatures. Before optical measurements the single crystals were cleaved by means of scotch tape and mounted on a cold finger of a liquid-He flow optical cryostat equipped with CaF_2 windows.

III. RESULTS

A. Experimental data

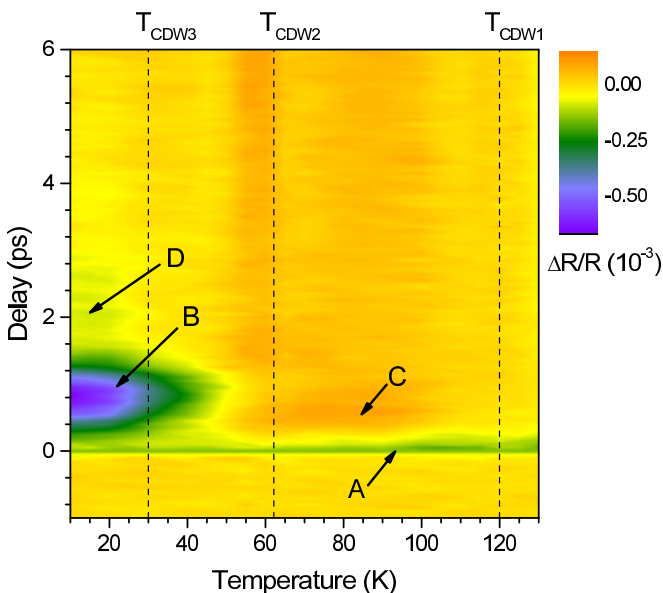


Figure 2. Temperature dependence of the transient reflectivity in $(\text{PO}_2)_4(\text{WO}_3)_{12}$ measured at the $8 \text{ }\mu\text{J}/\text{cm}^2$ pump fluence. Vertical dashed lines indicate the transition temperatures: $T_{\text{CDW}3} = 30 \text{ K}$, $T_{\text{CDW}2} = 62 \text{ K}$ and $T_{\text{CDW}1} = 120 \text{ K}$.

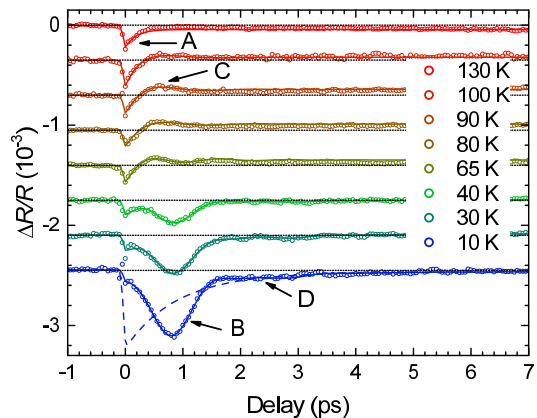


Figure 3. Transient reflectivity in $(\text{PO}_2)_4(\text{WO}_3)_{12}$ at selected temperatures recorded with $8 \text{ }\mu\text{J}/\text{cm}^2$ pump fluence. The transients are vertically shifted for clarity with the dotted lines indicating the shifts. The continuous lines are DCE-model fits discussed in text. The dashed line corresponds to the displaced equilibrium position for oscillators at 10 K. There is a notable coherent artifact due to the pump scattering appearing as increased noise at zero delay.

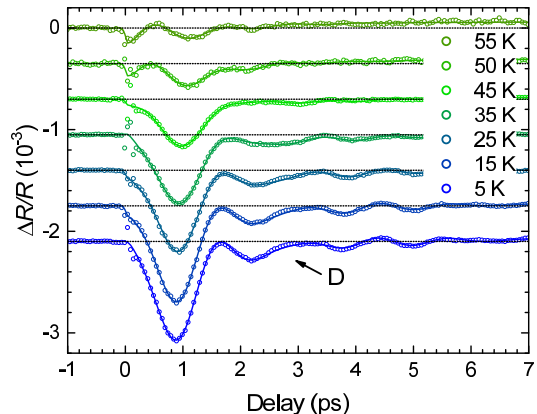


Figure 4. Transient reflectivity in $(\text{PO}_2)_4(\text{WO}_3)_{12}$ in the low- T region recorded with $8 \text{ }\mu\text{J}/\text{cm}^2$ pump fluence. The transients are vertically shifted for clarity with the dotted lines indicating the shifts. The continuous lines are DCE-model fits discussed in text. There is a notable coherent artifact due to the pump scattering appearing as increased noise at zero delay.

In Figs. 2, 3 and 4 we show the temperature dependence of the transient reflectivity $(\Delta R/R)$ in $(\text{PO}_2)_4(\text{WO}_3)_{12}$ taken at a pump fluence of $8 \text{ }\mu\text{J}/\text{cm}^2$. The response is characterized by four main features.

The first is a sub-picosecond negative transient (feature A), which changes only little with decreasing T .

The second and the most prominent is a larger picosecond negative transient (feature B) that appears on top of feature A below $T_{\text{CDW}2} = 62 \text{ K}$. Remarkably, feature B (Fig. 3) displays a risetime that appears slightly longer than the decay time.

The third is a small positive feature C (see Fig. 3)

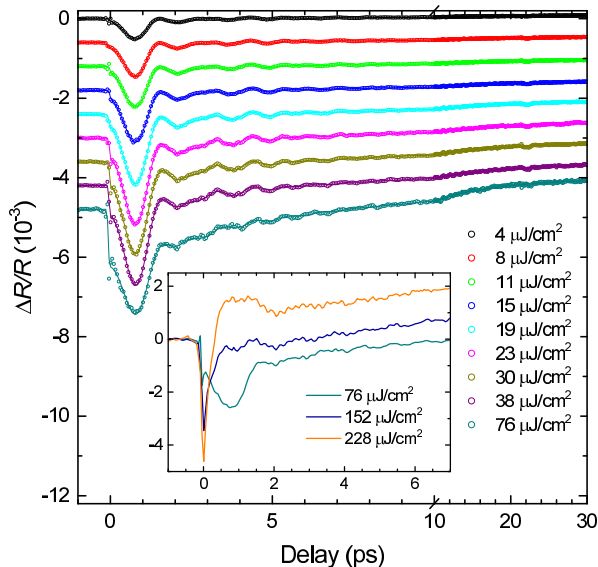


Figure 5. Pump fluence dependence of the transient reflectivity at 5 K. The traces are vertically shifted for clarity. The thin lines are the DCE-model fits discussed in text. The inset shows the qualitative change at the fluences above $76 \mu\text{J}/\text{cm}^2$.

peaked at ~ 0.5 ps that appears below $T_{\text{CDW}1} = 120$ K and develops into a weak oscillation when approaching $T_{\text{CDW}2}$.

The fourth is a negative shoulder together with additional weak oscillations beyond ~ 2 ps delay (feature D in Figs. 3 and 4), that appear below the lowest transition at $T_{\text{CDW}3} = 30$ K.

The feature-D weak oscillations were not completely reproducible between different experimental runs. While the T -dependence shown in Fig. 4 was measured in the first run immediately after cleaving the sample the data shown in Fig. 3 were measured in the second run after keeping the sample in vacuum for 12 days. Since it is not possible to measure exactly the same sample spot in different runs it is not clear whether the difference can be attributed to deterioration of the sample surface or surface inhomogeneity.

In Fig. 5 we plot the pump fluence dependence of the transient reflectivity measured at $T = 5$ K during the first run. The magnitude of the transients shows saturation with increasing \mathcal{F} above $\sim 20 \mu\text{J}/\text{cm}^2$. With further fluence increase the response changes qualitatively above $\mathcal{F} \simeq 80 \mu\text{J}/\text{cm}^2$ as shown in the inset of Fig. 5.

B. Analysis

An unusual feature of the data, which we need to understand, is that at the lowest temperatures the risetime of feature B apparently exceeds the decay time. Due to the ubiquitous appearance of a coherent collective oscillations in the transient reflectivity upon CDW formation⁴⁻⁶ it is very likely that the unusual shape of feature B is due

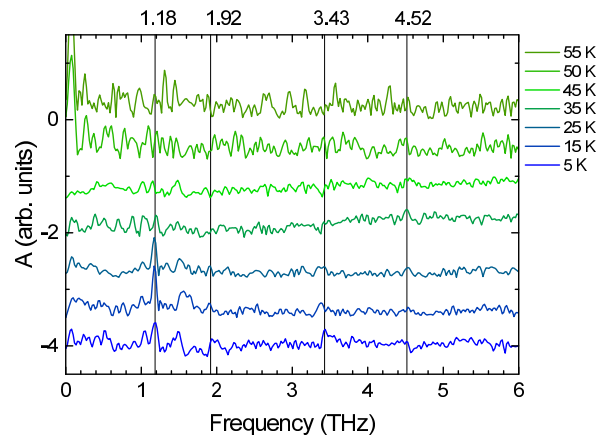


Figure 6. Fourier transforms of the T -dependent data in Fig. 4 with the DCE-model fits subtracted. The traces are vertically shifted and the main remaining coherent oscillation peaks are indicated by vertical lines.

to an interference between coherent oscillations. To test this hypothesis and get better insight into the unusual shape of feature B we fit the data using the theory of dispersive coherent excitation (DCE) of oscillatory modes²¹:

$$\begin{aligned} \frac{\Delta R}{R} = & (A_{\text{displ}} - \sum A_{O_i}) \int_0^\infty G(t-u) e^{-u/\tau_{\text{displ}}} du + \\ & + \sum A_{O_i} \int_0^\infty G(t-u) e^{-\gamma_i u} [\cos(\Omega_i u) - \\ & \quad - \beta_i \sin(\Omega_i u)] du + \\ & + \sum_{j \in \{1,2\}} A_{e_j} \int_0^\infty G(t-u) e^{-u/\tau_j} du, \end{aligned} \quad (1)$$

with $\beta_i = (1/\tau_{\text{displ}} - \gamma_i)/\Omega_i$ and $G(t) = \sqrt{2/\pi} \tau_p \exp(-2t^2/\tau_p^2)$. τ_p is the effective pump-probe pulse cross-correlation width, A_{O_i} , Ω_i , γ_i are oscillator amplitudes, frequencies and damping factors, respectively, while A_{e_j} and τ_j are amplitudes and relaxation times of the overdamped exponentially relaxing modes.

We also assume that all oscillators are driven by a single exponential term with relaxation time τ_{displ} , while the remaining exponential relaxations are kept independent from the oscillators. Note that the oscillator coordinates contain both the exponentially relaxing and oscillatory components.

It turns out that it is possible to fit the main features of the data using four oscillators at ~ 1 , ~ 0.8 , ~ 0.7 and ~ 0.5 THz with two independent exponential relaxations ($\tau_1 \sim 20$ ps and $\tau_2 \sim 10$ ns) in addition to the main relaxation component ($\tau_{\text{displ}} \lesssim 1$ ps) that drives the oscillators. Fourier transforms of the fit residua shown in Figs. 6 and 7 reveal additional four clearly resolvable modes at the lowest T .

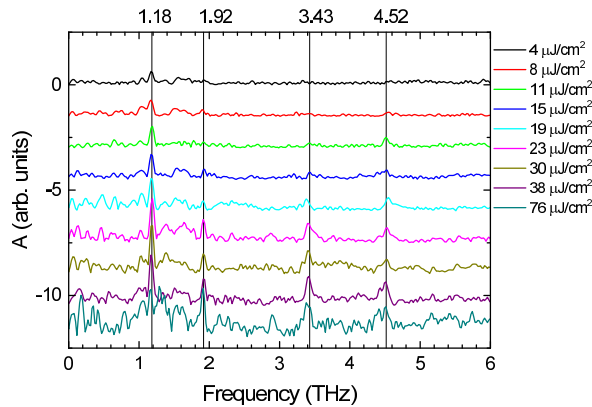


Figure 7. Fourier transforms of the fluence dependent data in Fig. 5 with the DCE-model fits subtracted. The traces are vertically shifted and the main remaining coherent oscillation peaks are indicated by vertical lines.

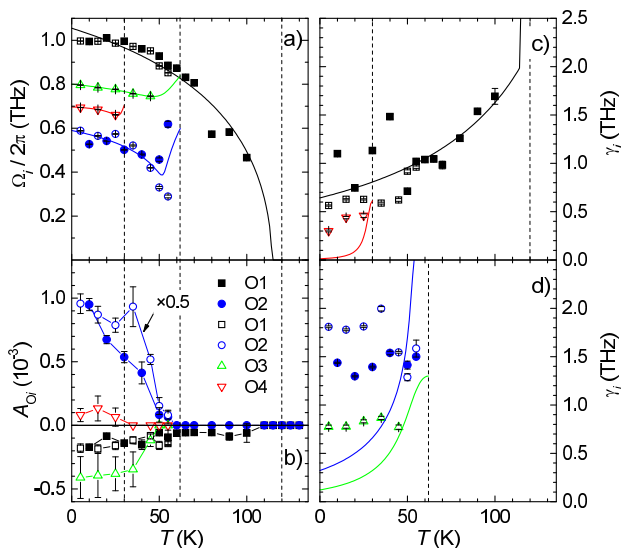


Figure 8. Temperature dependence of the oscillatory-modes DEC-model fit parameters. The continuous lines in (a), (c) and (d) are the TDGL theory^{7,22} fits. Full and open symbols represent data from two separate experimental runs from Figs. 3 and 4, respectively. The vertical dashed lines correspond to the three CDW transition temperatures.

IV. DISCUSSION

The presence of collective coherent oscillatory excitations in the photoinduced transient response of various CDWs is ubiquitous^{4–6,23–25} and comes from the coupling of phonons to the electronic order parameter which drives the transition⁷. In most cases several weakly damped coherent oscillations are observed well below the CDW transition temperatures, with widely different degrees of softening when approaching the transition from below.^{4–6,25,26} The softening has been parametrized using

mode	$\Omega_{\text{expt}}/2\pi$ (THz)	$\Omega_0/2\pi$ (THz)	a	T_{CDW} (K)
O1	1.0	1.6	2.8	120
O2	0.53	0.75	1.2	62
O3	0.79	0.79	0.3	62
O4	0.69	0.71	0.3	30

Table I. The TDGL fit parameters for the four main coherent oscillatory modes obtained from the fits in Fig. 8.

the time dependent Ginzburg-Landau (TDGL) theory^{7,22} by the adiabaticity ratio:

$$a = \kappa m^2 / \Omega_0^3, \quad (2)$$

where κ is the bare damping of the electronic mode, Ω_0 the bare phonon frequency and m the coupling between the electronic order parameter and the bare phonon mode. $a \gg 1$ corresponds to the adiabatic limit corresponding to the strongest degree of phonon softening. $a \sim 1$ corresponds to the non-adiabatic case with no softening and increased damping of the oscillatory component when approaching the transition temperature from below. In this case the soft mode is the critically damped solution dominated by the electronic order parameter.²²

In the case of $(\text{PO}_2)_4(\text{WO}_3)_{12}$ the main coherent oscillations at ~ 1 THz and ~ 0.5 THz appear strongly damped down to the lowest T with significantly weaker less-damped modes observed only below $T_{\text{CDW}3}$.

Despite being rather weak the 1-THz mode (O1) could be associated with the formation of CDW1 at $T_{\text{CDW}1}$. When approaching $T_{\text{CDW}1}$ from below (see Fig. 8) it softens by $\sim 50\%$ and with an increase of damping vanishes above ~ 100 K.

Below $T_{\text{CDW}2}$ two additional modes appear. The strongest is the ~ 0.5 -THz mode (O2) which shows $\sim 30\%$ softening with increasing T and vanishes above 55 K. Above 50 K the frequency shows large scatter between the two experimental runs, presumably due to a small amplitude and rather large damping that couples the fit parameters of modes O1 and O2. The second mode at ~ 0.8 THz (O3) is weaker, but less damped with a softening of less than 10% disappearing above $T \sim 50$ K.

Below $T_{\text{CDW}3}$ another two modes appear. The strongest ~ 0.7 THz mode (O4) shows $\sim 5\%$ softening with increasing T , while the weaker one at ~ 1.2 THz, that was not included in fits (see Figs. 6 and 7) shows virtually no softening.

The three higher frequency modes observed clearly at higher fluences (see Fig. 7) can not be clearly associated with any of the transitions due to the weak intensities at the pump fluence used for the T scans.

The T dependence of the mode frequencies is consistent with predictions of the TDGL model^{7,22} as shown in Fig. 8 (a). However, except for mode O1 [see Fig. 8(c) and (d)] it is not possible to obtain simultaneous good fits for damping. The experimental dampings greatly exceed

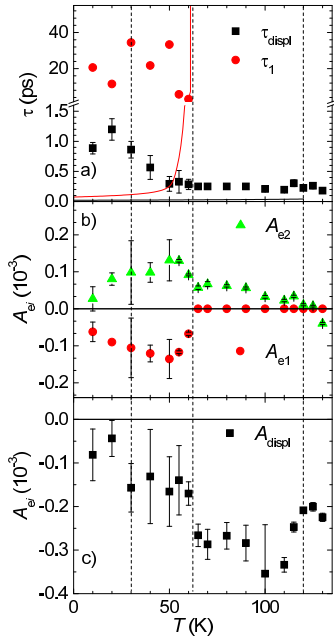


Figure 9. Temperature dependence of the exponential-modes DCE-model fit parameters from Fig. 3. The red continuous line in (a) is the TDGL theory^{7,22} prediction corresponding to the mode-O2 fit in Fig. 8. The vertical dashed lines correspond to the three CDW transition temperatures.

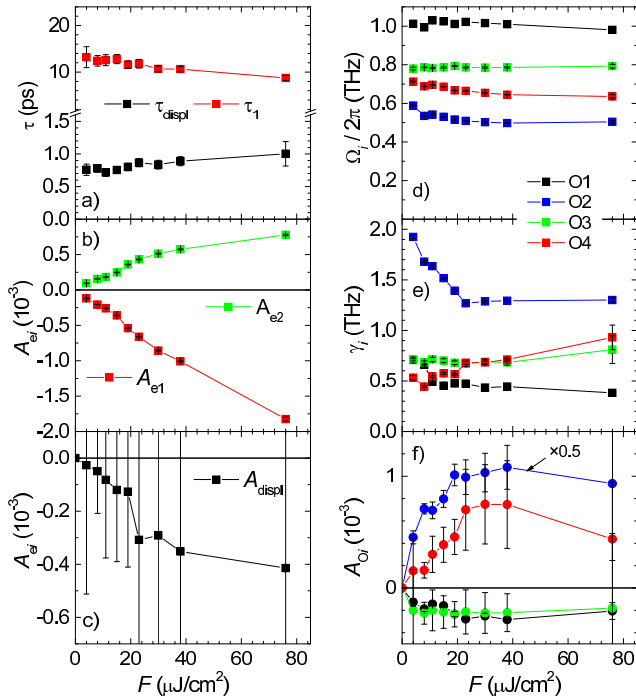


Figure 10. Fluence dependence of the DCE-model fit parameters at $T = 5$ K from Fig. 5. The large error bars in (c) are due to the small amplitude of the displacive component in comparison to the oscillator components amplitudes.

the model predictions for modes O2, O3 and O4, except near the CDW transitions, where the model dampings increase. We attribute excess damping at lower T to the combination of extrinsic and intrinsic phonon damping that is not directly related to the CDWs and is not included in the TDGL model^{7,22}. The model also predicts a region of critical damping for mode O1 just below T_{CDW1} which is due to the vanishing amplitude experimentally inaccessible.

The main TDGL-theory parameters are shown in Table I. The bare frequencies of modes O1 and O2 appear strongly renormalized by the coupling to the electronic order parameter, while the renormalization is small for the other modes.

The model⁷ also predicts a second critically damped mode, that is weakly T -dependent in the adiabatic case and softens at T_{CDW} in the non-adiabatic case. For CDW1 the mode-O1 fit in Fig. 8 (a) and (c) implies a fast virtually T -independent mode with $\tau \sim 20 - 50$ fs, which is ten times faster than the fastest observed relaxation. If the excitation goes through a displacive mechanism involving electrons in the ungapped bands the fast mode would adiabatically follow the displacive drive resulting in the response consistent with the data.

In contrast, for CDW2 and CDW3 the fits to modes O2, O3 and O4 in Fig. 8 (a) imply overdamped soft modes with rather fast relaxation times diverging at the corresponding T_{CDW} as shown for mode O2 by the red solid line in Fig 9 (a). None of the three observed exponential relaxation components (τ_{disp} , τ_1 , and τ_2) show such a divergence and therefore cannot be directly associated with the overdamped part of the order parameter dynamics. This indicates that photons at the energy used in the present experiment (1.55 eV) are only weakly coupled to the electronic order parameters associated with CDW2 and CDW3.

The present behaviour is different from observations⁸ in structurally similar²⁷ η - Mo_4O_{11} where a diverging relaxation time of the overdamped soft mode is clearly observed while the phonon modes associated with the CDW formation show virtually no softening when approaching the CDW transition temperature. This is consistent with the non-adiabatic limit of the TDGL theory. One of the reasons for a smaller adiabaticity ratio a [see Eq. (2)] could be higher frequencies of the CDW related modes (1.93, 2.19 and 2.94 THz) in η - Mo_4O_{11} originating in the smaller Mo mass.

Looking at the pump fluence dependence of the DCE-model fit parameters in Fig. 10 we observe a clear saturation of the coherent-oscillatory-mode amplitudes above $\mathcal{F}_{\text{sat}} \sim 20 \mu\text{J}/\text{cm}^2$ while the amplitudes of the exponential relaxation components show only a slightly sublinear behavior. Surprisingly, within error bars the amplitudes of all the oscillatory modes²⁸ saturate at the same fluence. Except for the damping of the strongest mode O2 the other coherent-oscillatory-mode parameters also show no strong changes around \mathcal{F}_{sat} and remain nearly constant up to $\mathcal{F} \sim 80 \mu\text{J}/\text{cm}^2$.

Previously it has been shown that increasing the pump fluence transiently suppresses and eventually destroys the CDW order.^{23–25,29} Since in our experiment the CDW-induced modes remain clearly visible up to $\mathcal{F} \sim 80 \mu\text{J}/\text{cm}^2$ and are completely suppressed only at higher fluences the saturation at \mathcal{F}_{sat} can not be attributed to the complete destruction of CDWs. It is however unusual, that even the amplitude of mode O4 associated with the weakest CDW3 shows only a moderate additional suppression with increasing \mathcal{F} above \mathcal{F}_{sat} .

A similar behavior in $1T\text{-TiSe}_2$, where the periodic lattice distortion (PLD) persists upon destruction of the electronic ordering, has been attributed³⁰ to sequential suppression of the electronic excitonic component of the CDW order at a lower and the Jahn-Teller component at a higher pump fluence. In the case of $(\text{PO}_2)_4(\text{WO}_3)_{12}$ it is believed that the CDWs are well described in the framework of the Pirls-like mechanism with "hidden" nesting vectors.^{9,10} In this picture the PLD and the electronic part of the order parameter work in conjunction to form CDWs. However, on a short timescale they can become decoupled due to their different intrinsic timescales. The saturation of the coherent-oscillatory-mode amplitudes can be therefore attributed to such decoupling. In the case when the electronic parts of CDWs are transiently completely suppressed and partially recover on a timescale $\tau_{\text{rec}} \ll \Omega_i^{-1}$ the PLDs can not be completely suppressed. The rather short relaxation times, $\tau_i \lesssim 100$ fs, of the overdamped modes suggested by the TDGL model fits are consistent with such scenario.

Independently of the above saturation scenario the decrease of the mode O2 damping with increasing fluence below \mathcal{F}_{sat} could be attributed to the inhomogeneous excitation profile. Due to the finite light penetration depth the CDWs are more strongly suppressed near the surface. The relative contribution of the near-surface part of the excited volume to the response is therefore decreased leading to a decrease of damping in the case of an enhanced extrinsic damping of the mode due the surface effects.

V. SUMMARY AND CONCLUSIONS

We investigated the effect of a sequence of three consecutive CDW transitions in a mono-phosphate tungsten

bronze $(\text{PO}_2)_4(\text{WO}_3)_{2m}$ ($m = 6$) on the photoinduced ultrafast transient coherent oscillatory optical response. We clearly observe the appearance of new coherent oscillatory modes below each CDW transition. At low T the interference of two rather strongly damped modes at ~ 1 and ~ 0.5 THz, which can be associated with CDW1 at 120 K and CDW2 at 62K, respectively, leads to an unusual *rectified* transient reflectivity with an inverted-Gaussian shape.

The T -dependence of the coherent mode frequencies can be well described in the framework of the recently proposed TDGL model^{7,22}. The damping of the most strongly coupled mode at ~ 1 THz, which is coupled with CDW1 order parameter, is consistent with the TDGL model. On the other hand, the less strongly coupled modes associated with CDW2 and CDW3 show an additional intrinsic damping that does not originate from the coupling to the electronic order parameters.

Contrary to the oscillatory modes, no corresponding overdamped modes predicted by the TDGL model are observed using probe photons at 1.5 eV, which may be explained to be due to weak coupling between the 1.55-eV photons and the electronic parts of the respective order parameters. Further broad-band-probe transient reflectivity studies would be necessary to possibly reveal the overdamped modes.

With increasing the pump fluence we observe a saturation of the coherent mode amplitudes well below the complete destruction of the CDWs. This could be attributed to a decoupling of the electronic and lattice parts of the order parameter resulting in a complete ultrafast transient suppression and a partial recovery of the electronic part of the order parameter on a timescale much shorter than the coherent-mode periods.

VI. ACKNOWLEDGMENTS

The authors acknowledge Slovenian Ministry of education, science and sport (project ULTRA-MEM-DEVICE No. PR-05665), Slovenian Research Agency and European Research Council advanced grant TRAJECTORY for financial support. We acknowledge D. Groult and Ph. Labbé at CRISMAT (Caen, France) for providing the samples. We would like to thank also P. Gubelj for helping with the optical measurements and V.V. Kabanov and J. Demsar for fruitful discussions.

* tomaz.mertelj@ijs.si

¹ G. Travaglini, I. Mörke, and P. Wachter, Solid State Communications **45**, 289 (1983).

² S. Sugai, physica status solidi (b) **129**, 13 (1985).

³ M. Lavagnini, H.-M. Eiter, L. Tassini, B. Muschler, R. Hackl, R. Monnier, J.-H. Chu, I. Fisher, and L. Degiorgi, Physical Review B **81**, 081101 (2010).

⁴ J. Demsar, K. Biljaković, and D. Mihailovic, Phys. Rev. Lett. **83**, 800 (1999).

⁵ K. Shimatake, Y. Toda, and S. Tanda, Phys. Rev. B **75**, 115120 (2007).

⁶ R. V. Yusupov, T. Mertelj, J. h. Chu, I. R. Fisher, and D. Mihailovic, Phys. Rev. Lett. **101**, 246402 (2008).

⁷ H. Schäfer, V. V. Kabanov, M. Beyer, K. Biljakovic, and J. Demsar, Phys. Rev. Lett. **105**, 066402 (2010).

- ⁸ M. Borovšak, L. Stojchevska, P. Sutar, T. Mertelj, and D. Mihailovic, *Physical Review B* **93**, 125123 (2016).
- ⁹ P. Foury, J. P. Pouget, E. Wang, and M. Greenblatt, *Europhys. Lett.* **16**, 485 (1991).
- ¹⁰ P. Foury and J. P. Pouget, *International Journal of Modern Physics B* **7**, 3973 (1993).
- ¹¹ P. Roussel, O. Perez, and P. Labbe, *Acta Crys B* **57**, 603 (2001).
- ¹² P. Foury and J. P. Pouget, *Solid State Sciences* **4**, 387 (2002).
- ¹³ V. V. S. et al., *Russian Chemical Reviews* **73**, 753 (2004).
- ¹⁴ C. Schlenker, C. Hess, C. Le Touze, and J. Dumas, *Journal de Physique I* **6**, 2061 (1996).
- ¹⁵ M. Greenblatt, "Physics and chemistry of low-dimensional inorganic conductors," (Springer Science & Business Media, 1996) Chap. 2, p. 15.
- ¹⁶ E. Wang, M. Greenblatt, I. E. Rachidi, E. Canadell, M. H. Whangbo, and S. Vadlamanti, *Phys. Rev. B* **39**, 12969 (1989).
- ¹⁷ C. Schlenker, *Low-Dimensional Electronic Properties of Molybdenum Bronzes and Oxides* (Kluwer Academic Press, Dordrecht, 1989).
- ¹⁸ M. Greenblatt, *International Journal of Modern Physics B* **7**, 3937 (1993).
- ¹⁹ C. Schlenker, "Physics and chemistry of low dimensional inorganic conductors," (Plenum Press, New York, 1996) Chap. 8, p. 115.
- ²⁰ B. R. Ph. Labbé, M. Goreaud, *J. Solid State Chem* **62** (1986), 324.
- ²¹ H. Zeiger, J. Vidal, T. Cheng, E. Ippen, G. Dresselhaus, and M. Dresselhaus, *Physical Review B* **45**, 768 (1992).
- ²² H. Schaefer, V. V. Kabanov, and J. Demsar, *Physical Review B* **89**, 045106 (2014).
- ²³ F. Schmitt, P. S. Kirchmann, U. Bovensiepen, R. G. Moore, L. Rettig, M. Krenz, J.-H. Chu, N. Ru, L. Perfetti, D. H. Lu, M. Wolf, I. R. Fisher, and Z.-X. Shen, *Science* **321**, 1649 (2008), <http://science.sciencemag.org/content/321/5896/1649.full.pdf>.
- ²⁴ L. Perfetti, P. A. Loukakos, M. Lisowski, U. Bovensiepen, M. Wolf, H. Berger, S. Biermann, and A. Georges, *New Journal of Physics* **10**, 053019 (2008).
- ²⁵ A. Tomeljak, H. Schäfer, D. Städter, M. Beyer, K. Biljakovic, and J. Demsar, *Phys. Rev. Lett.* **102**, 066404 (2009).
- ²⁶ J. Demsar, L. Forro, H. Berger, and D. Mihailovic, *Phys. Rev. B* **66**, 041101 (2002).
- ²⁷ Both compounds contain similar octahedral layers separated by tetrahedral units, but with different stacking.
- ²⁸ The amplitude of mode O3 appears saturated below the lowest measured pump fluence. We believe that this is a fit artifact due to a strong correlation of the fit amplitude with mode O4, which has a very similar frequency, but the opposite phase.
- ²⁹ R. Yusupov, T. Mertelj, V. V. Kabanov, S. Brazovskii, P. Kusar, J.-H. C. Chu, I. R. Fisher, and D. Mihailovic, *Nature Physics* **6**, 681 (2010).
- ³⁰ M. Porer, U. Leierseder, J.-M. Ménard, H. Dachraoui, L. Mouchliadis, I. Perakis, U. Heinzmann, J. Demsar, K. Rossnagel, and R. Huber, *Nature materials* **13**, 857 (2014).